TRIBOLOGY INTERNATIONAL (FRANCE/USA)

Impact factor = 5.62

Accepted May 17th 2023

Functional magnetic Maxwell viscoelastic nanofluids for tribological coatings- *a model for stretching flow using the generalized theory of heat-mass fluxes, Darcy-Forchheimer formulation and dual convection*

Muhammad Nasir[1], M. Waqas[2,3,*] O. Anwar Bég[4], Sami Znaidia[5], W. A. Khan[6] and Nurnadiah Zamri[1]

[1]*Faculty of Informatics and Computing, University Sultan Zainal Abidin, Besut Campus, 22200 Besut, Tereng-ganu, Malaysia*
[2]*NUTECH School of Applied Science and Humanities, National University of Technology, Islamabad 44000, Pakistan*
[3]*Department of Mechanical Engineering, Lebanese American University, Beirut, Lebanon*
[4]*Professor and Director-Multi-Physical Engineering Sciences Group, Mechanical Engineering, Salford University, School of Science, Engineering and Environment (SEE), Manchester, M54WT, UK*
[5]*College of Sciences and Arts in Mahayel Asir, Department of Physics, King Khalid University, Abha, Saudi Arabia.*
[6]*School of Mathematics and Statistics, Beijing Institute of Technology, Beijing 100081, China*
**Correspondence:* muhammadwaqas@nutech.edu.pk *(M. Waqas)*

Abstract: A theoretical and computational study of *an improved Fourier and Fickian model for locally non-similar magnetohydrodynamic Maxwell (non-Newtonian) nanofluid convective flow under thermo-solutal buoyancy forces in a non-Darcian (*Darcy-Forchheimer) *porous medium is presented*. Heat sink/source is included. Buongiorno's two-component nanofluid model is used to simulate nanoscale characteristics featuring thermophoresis and Brownian diffusions. The problem under consideration is formulated utilizing fundamental relations of fluid dynamics. The primitive partial differential expressions (PDEs) are transfigured to ordinary ones with apposite transformations. The emerging locally non-similar boundary value problem is solved via series expansions utilizing a homotopy algorithm. Characteristics of sundry parameters on velocity, temperature, nanoparticle concentration and skin-friction coefficients are interpreted graphically. Convergence results acquired via homotopy algorithm are presented. Comparison results are included for the authentication of the homotopy solutions. The velocity distribution is increased with greater mixed convection and non-Newtonian material parameters whereas velocity distribution is reduced with increment in Hartmann (magnetic) number, porosity and buoyancy ratio parameters. The temperature distribution is reduced when Prandtl number and thermal-relaxation (non-Fourier) parameter are augmented whereas temperature distribution is increased for larger Brownian diffusion and thermophoresis. Additionally, it is observed that increment in the heat absorption variable diminishes temperature whereas an enhancement in the heat generation variable augments temperature. Nanoparticle concentration is enhanced subjected to higher values of thermophoresis factor whereas it reduces with larger Schmidt number, Brownian movement and solutal-relaxation (non-Fickian) parameters. Furthermore, it is noticed that elevation in Hartmann number, porosity and inertial (non-Darcy) coefficient parameters increase the skin friction coefficient whereas elevation in Deborah number and buoyancy ratio is found to suppress skin friction. The simulations are relevant to hydromagnetic nano-materials processing operations for coatings deployed in multi-functional tribological systems and surface protection.

Keywords: *Non-Fourier; non-Fickian; magnetohydrodynamics; Darcy-Forchheimer porous media; Maxwell viscoelastic nanofluid; Heat sink/source; Homotopy algorithm; non-classical non-similar symmetry; magnetic nano-materials processing.*

Nomenclature

Fr	Forchheimer inertia coefficient parameter;	D_B	Brownian diffusion coefficient ($\mathrm{m^2.s^{-1}}$);
D_t	Thermophoretic diffusion coefficient ($\mathrm{m^2.s^{-1}}$);	u, v	velocity components ($\mathrm{ms^{-1}}$);
δ_2	Solutal relaxation parameter;	C_f	Skin friction coefficient;
S	heat generation/absorption;	δ_1	Thermal relaxation parameter;
T	Fluid temperature (K);	Re_x	Local Reynolds number;
$\Pr$	Prandtl number;	θ	Dimensionless temperature;
λ_1	mixed convection parameter;	ϕ	Dimensionless concentration;
β	Deborah number;	ρ_f	Density of base-fluid ($\mathrm{kgm^{-3}}$);
C_∞	Ambient fluid concentration (Moles);	Sc	Schmidt number
T_∞	Ambient fluid temperature (K);	f	Dimensionless velocity;
λ	Darcian permeability parameter;	N_t	Thermophoresis parameter;
N_b	Brownian motion parameter;	N	buoyancy ratio;
η	Similarity variable;	x, y	coordinate axes (m)

1. Introduction

Heat and mass transport processes feature in a diverse spectrum of engineering and industrial systems including power generation, energy production, pharmaceutical synthesis, refrigeration, cooling of atomic reactors, tribology, heat exchangers and materials fabrication. Scientists simulating thermo-solutal transport processes have generally established mathematical models under the classical theories of Fourier thermal conduction and Fickian mass diffusion. These theories are insufficient where more complex energy and concentration relaxation aspects are involved in many engineering problems. In providing more refined estimates of thermal and mass characteristics in for example materials processing, it is important to incorporate non-Fourier and non-Fickian methodologies. Keeping in mind such significance, Cattaneo [1] introduced the idea of "thermal relaxation." To improve Fourier's parabolic heat conduction theory which ignores thermal waves, he developed the so-called hyperbolic Maxwell-Cattaneo law. Christov [2] further worked on the Cattaneo model to improve this theory and introduced the upper-convected derivative formulation. A similar refinement in mass diffusion physics based on the classical Fickian approach has also taken place leading to *non-Fickian* formulations which feature solutal relaxation effects. Subsequently many researchers have adopted these improved approaches to study more precisely the heat and species diffusion in a range of industrial flow problems for both Newtonian and non-Newtonian fluent media. Ijaz *et al.* [3] computed the effects of Cattaneo–Christov heat-mass flux models on Walters-B viscoelastic squeezing lubrication transport. They solved nonlinear systems using a shooting technique and concluded that thermal and solutal relaxation effects result in a decline of the temperature along with concentration of the squeezed motion. Hafeez *et al.* [4] deployed the modified Fourier and Fick diffusion models for swirling flow from a rotating disk with heat generation/absorption. Analytical series solutions were obtained by applying the homotopic approach and verified with numerical approaches. Rawat *et al.* [5] numerically examined the Oldroyd-B nanoliquid flow across an elongating surface in the presence of activation energy via RKF (Runge–Kutta–Fehlberg) shooting scheme with modified Fourier and Fickian diffusion models. They showed that temperature decreases with growing thermal relaxation parameter. Further, Haider *et al.* [6] scrutinized the impact of the non-Fickian and non-Fourier models on the time-independent 2D flow of second grade nanoliquid towards an extending sheet by via Bvp4c in MATLAB. Chu *et al.* [7] computed double-diffusive non-Fourier/Fickian convection in Maxwell nano liquid with Stefan blowing and bioconvection. Khan *et al.* [8] inspected the magnetized viscous nanoliquid flow with convective boundary conditions using the non-Fickian and non-Fourier diffusion theories. Their examination was focused on numerous geometries (cone, wedge, and plate). They reported that thermal and solutal relaxation factors induce a decreasing trend against temperature and solutal characteristics. Ibrahim and Gadisa [9] evaluated the characteristics of Fourier and Fickian diffusion on Oldroyd-B fluid with heat source/sink using a Galerkin finite element technique (GFEM). Khan *et al.* [10] explored the influence of the non-Fickian and non-Fourier solutal and thermal relaxation effects on the Williamson fluid flow from an elastic surface in porous media under a magnetic field. Thy showed that velocity and concentration distributions show opposing behavior for Fourier thermal and Fickian solutal relaxation time variables.

Analysis of heat transport in viscous flow from a stretchable surface (linearly or nonlinearly extending) has stimulated considerable attention as it is fundamental to materials fabrication technologies which are important in the manufacture of various functional materials of use in for example, modern tribology. Examples include coating deposition, extrusion of polymer sheets, fiber spinning, injection moulding, plastic and rubber sheet synthesis, metallurgical purification, chocolate and toffee manufacture and galvanic finishing of metallic surfaces in a bath. Crane [11] initiated the mathematical modelling of fluid flows induced by the stretching of a sheet. Subsequently many investigators extended Crane's Newtonian model to consider a multiplicity of effects including magnetic fields, heat transfer, mass transfer, non-Newtonian liquids and complex surfaces. which was later extended by other researchers. Models have increasingly become more refined to embrace the novel materials synthesized by engineers including smart polymers, functional nanomaterials and intelligent coatings. These materials feature responsiveness to external magnetic fields, complex rheology and nanoparticle embedding. Via the use of bespoke metallic nanoparticles, special characteristics can be achieved and performance in engineering systems can be enhanced. Jafarimoghaddam [12] simulated the magnetized Maxwell nanoliquid porous flow of along a bidirectional moving surface with convective boundary layer conditions. Recently, Habib *et al.* [13] scrutinized the comparative behaviour of different non-Newtonian constitutive models (Williamson, micropolar and Maxwell) in polymer dynamics from a stretchable surface with double diffusion and activation energy effects. Prasannakumara [14] performed a numerical simulation of the flow of functional electro-conductive Maxwell nanofluids with magnetic dipole effects from an extending sheet. Many different numerical and semi-numerical approaches have been deployed in solving the nonlinear boundary-layer flows characterizing multi-physical stretching sheet transport phenomena. Sequential linearization methods were utilized by Daoud *et al*. [15] to study the boundary-layer flow of viscous fluid across a stretchable surface. Furthermore, Kumar *et al.* [16] used Runge-Kutta numerical quadrature to compute the flow of upper-convected Maxwell nanoliquid confined by extending sheet under the impact of a magnetic dipole. Recently, numerous articles regarding the study of stretchable boundary flows for a wide spectrum of chemo-physical and magnetic effects have been communicated [17-22].

A major improvement in 21st century functional materials has been the emergence of nanotechnology-based heat transport liquids. Nanofluids have become very popular as nanoengineered colloidal suspensions and were developed by Choi and Eastman [23] to develop the thermal conductivity and performance of ordinary fluids. They have been deployed in many technologies including biomedicine, coating, renewable energy, environmental protection and propulsion systems. Many theoretical and computational studies of nanofluids have therefore appeared in the literature in recent years. These have addressed both Newtonian and non-Newtonian behaviour, the latter important due to the doping effect of nanoparticles which can alter the rheology of suspensions. The dynamics of Carreau nanofluids across a stretching surface was investigated numerically by Eid *et al*. [24]. Furthermore, heat source/sink and mixed convection on the $Cu - Al_2O_3 - H_2O$ hybrid nanoliquid via permeable medium toward an elongating/shrinking sheet were inspected by Jamaludin *et al.* [25], who showed that local Nusselt number is modified strongly with copper nanoparticle doping. Salawu *et al.* [26] evaluated the hydromagnetic reactive Maxwell nanoliquid streaming flow induced by extending and nonlinear thermophysical properties. Some further recent studies of nanofluid mechanics are documented in Refs. [27-42].

Mixed convection flow includes a combination of free and forced convection. It arises in a range of technical and industrial procedures comprising nuclear reactors, fan-cooled electronic devices, drying, lubrication processes, wind current-exposed solar central receivers, heat exchangers mounted in low-velocity environments and also nanomaterials fabrication. Recently Qaiser *et al.* [43] scrutinized the mixed convection flow of Walters-B nanofluid with chemical reaction and Newtonian heating across an extending surface. The non-Newtonian mixed convection nanofluid transport from a permeable stretchable surface was examined numerically by Patil *et al.* [44]. Puneeth *et al.* [45] studied the 3D dual convective hybrid Casson nanoliquid flow across a stretching sheet. Mixed convection in hybrid nanofluids flow across stretching and shrinking sheets were examined by Waini *et al.* [46] who confirmed that when nanoparticles are incorporated, the heat transfer rate increases. Additional inquiries on the mixed convection in a variety of nanofluid configurations are provided in [47-49].

The above-mentioned literature did not consider improved Fourier and Fickian analysis and nonlinear rheological nanofluid characteristics in porous media adjacent to a stretchable surface. This regime is of considerable importance in the manufacture of modern tribological coatings which are instrumental in mitigating and controlling wear effects. The precision synthesis of thin film ionic and magnetic coatings via stretching and electromagnetic field tuning successfully modifies superficial properties without affecting the basic bulk material characteristics, as noted by Suleiman [50]. In particular, functional rheological nano-coatings can be produced to improve the hardness and toughness of the substrate surface and can be adapted strategically via adjusting the stretching rate to improve durability, friction, and/or wear characteristics [51-57]. These complex lubricants during and subsequent to extrusion manufacturing feature a plethora of multi-physics effects which require sophisticated models for their simulation.

Motivated therefore by evolving a more comprehensive model featuring Fourier and Fickian diffusion for nonlinear rheological nanofluids, as a simulation of functional nanomaterial coating operations, the present work simulates using *an improved Fourier and Fickian analysis the hydromagnetic reactive Maxwell viscoelastic nanoliquid flow via vertical stretchable surface to a non-Darcian permeable medium under thermo-solutal buoyancy forces.* The non-Fickian and non-Fourier diffusion formulations are deployed for the conservation of energy and species. The innovation of present research is thus the simultaneous deliberation of multiple effects, i.e., *Cattaneo–Christov heat-mass flux, non-Darcy permeable medium drag, heat generation/absorption, mixed convection, magnetic body force and non-Newtonian nanofluid characteristics on vertical stretching surface flow.* A boundary layer formulation is utilized. A boundary layer approach is used which was originally based on symmetry in the parabolic Prandtl boundary layer equations. Non-classical symmetry was emphasized in the Sparrow-Yu approach. This is the approach adopted in this research work. To solve the dimensionless ordinary differential expressions, an analytical method is used, i.e., the homotopy analysis method (HAM) [58-62]. Graphical and tabular results are utilized to show the influence of various control variables on momentum, heat transfer and nanoparticle mass heat transfer characteristics. Validation with previous simpler models is also included. Furthermore, a convergence assessment is conducted for the HAM solutions. A comparison of HAM with earlier literature is also included. Extensive interpretation of the results is presented.

2. Mathematical model for tribological magnetic nano-coating flow

Laminar, steady state magnetohydrodynamic (MHD) thermo-solutal non-similar mixed convective Maxwell non-Newtonian nanoliquid from a vertically stretchable surface subject to revised diffusion aspects (Cattaneo-Christov heat-mass flux) is considered. The vertical surface stretches with linear velocity $u_w(x) = cx$ (where c represents stretching rate constant). The *x*-axis is in direction of stretching of the vertical sheet and the y-axis is normal to it. Darcy's model is used to simulate the effect of bulk matrix drag in the porous medium. Thermal and solutal relaxations are taken into account. The model also includes the heat generation/absorption effect. The two-component Buongiorno model is deployed which is based on the consideration of a number of slip mechanisms between the nanoparticles and base liquid. It emphasizes the nanoparticle haphazard (Brownian dynamics) movement and thermophoresis under temperature gradient which controls the migration of nanoparticles from hotter zones to cooler zones. It is highly compatible with the boundary layer framework and the two main parameters are representative of actual nanoscale phenomena. Larger values of Brownian motion parameter physically imply smaller nanoparticle diameters which influences micro-convection around the nanoparticles and globally affects thermal diffusion in the nanofluid. The non-Newtonian nanofluid is electrically conducting owing to magnetic nanoparticle doping and a transverse magnetic field is imposed. Hall current, electrical polarization and magnetic induction effects are neglected. Under the above assumptions, the conservation equations for mass, momentum, energy and concentration of nanoparticles, using the Buongiorno nanofluid model, may be derived by extending the analysis of Turkyilmazoglu [63] and Sadiq and Hayat [64]. The regime studied is visualized in **Figure 1** and is relevant to nano-materials fabrication processing.

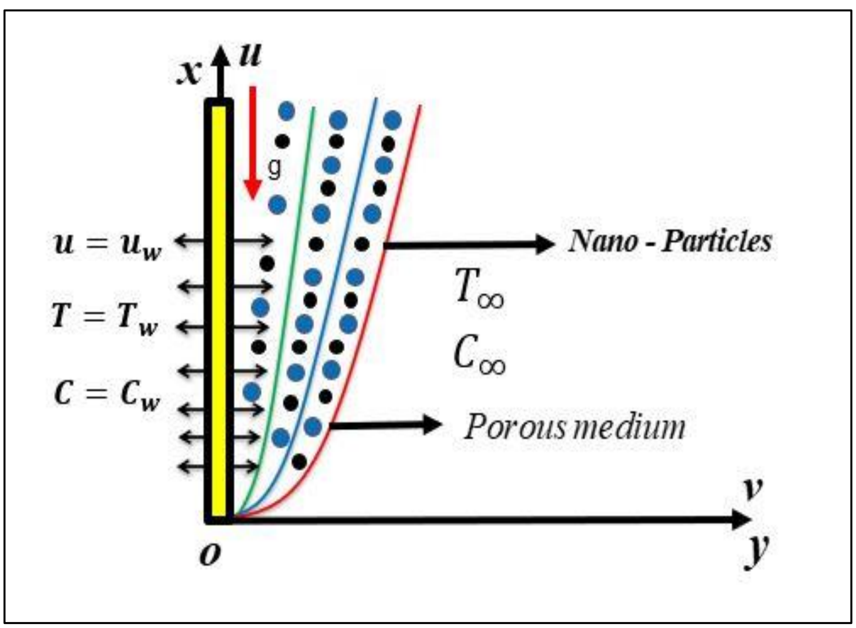

Fig. 1. Flow configuration model.

$$\frac{\partial u}{\partial x}+\frac{\partial v}{\partial y}=0, \tag{1}$$

$$u\frac{\partial u}{\partial x}+v\frac{\partial u}{\partial y}+\lambda_1\left(u^2\frac{\partial^2 u}{\partial x^2}+v^2\frac{\partial^2 v}{\partial y^2}+2uv\frac{\partial^2 u}{\partial x\partial y}\right)=\nu\frac{\partial^2 u}{\partial y^2}-\frac{\nu}{K}u-Fu^2-\frac{\sigma B_0^2}{\rho}\left(u+\lambda v\frac{\partial u}{\partial y}\right)+g\left(\beta_T\left(T-T_\infty\right)+\beta_C\left(C-C_\infty\right)\right), \tag{2}$$

$$\begin{cases} u\dfrac{\partial T}{\partial x}+v\dfrac{\partial T}{\partial y}=\alpha\dfrac{\partial^2 T}{\partial y^2}-\lambda_t\begin{bmatrix}\dfrac{\partial T}{\partial x}\left(u\dfrac{\partial u}{\partial x}+v\dfrac{\partial u}{\partial y}\right)+\dfrac{\partial T}{\partial y}\left(u\dfrac{\partial u}{\partial x}+v\dfrac{\partial u}{\partial y}\right)\\ +2uv\dfrac{\partial^2 T}{\partial x\partial y}+u^2\dfrac{\partial^2 T}{\partial x^2}+v^2\dfrac{\partial^2 T}{\partial y^2}\end{bmatrix}\\ +D_B\lambda_t\tau\left[u\dfrac{\partial^2 C}{\partial x\partial y}\dfrac{\partial T}{\partial y}+u\dfrac{\partial C}{\partial y}\dfrac{\partial^2 T}{\partial x\partial y}+v\dfrac{\partial^2 C}{\partial y^2}\dfrac{\partial T}{\partial y}+v\dfrac{\partial C}{\partial y}\dfrac{\partial^2 T}{\partial y^2}\right]\\ +2\lambda_t\tau\dfrac{D_T}{D_\infty}\left[u\dfrac{\partial T}{\partial y}\dfrac{\partial^2 T}{\partial x\partial y}+v\dfrac{\partial^2 T}{\partial y^2}\dfrac{\partial T}{\partial y}\right]+\dfrac{Q_0}{\left(\rho c\right)_f}\left(T-T_\infty\right)+\dfrac{Q_0}{\left(\rho c\right)_f}\lambda_t\left[u\dfrac{\partial T}{\partial x}+v\dfrac{\partial T}{\partial y}\right], \end{cases} \tag{3}$$

$$\begin{cases} u\dfrac{\partial C}{\partial x}+v\dfrac{\partial C}{\partial y}=D_B\dfrac{\partial^2 C}{\partial y^2}-\lambda_c\begin{bmatrix}\dfrac{\partial C}{\partial x}\left(u\dfrac{\partial u}{\partial x}+v\dfrac{\partial u}{\partial y}\right)+\dfrac{\partial C}{\partial y}\left(u\dfrac{\partial u}{\partial x}+v\dfrac{\partial u}{\partial y}\right)\\ +2uv\dfrac{\partial^2 C}{\partial x\partial y}+u^2\dfrac{\partial^2 C}{\partial x^2}+v^2\dfrac{\partial^2 C}{\partial y^2}\end{bmatrix}\\ -\dfrac{D_T}{D_\infty}\left[u\dfrac{\partial^3 T}{\partial x\partial y^2}+v\dfrac{\partial^3 T}{\partial y^3}+\dfrac{\partial^2 T}{\partial y^2}\right], \end{cases} \tag{4}$$

$$u=u_w\left(x\right)=cx,\ v=0,\ T=T_w,\ C=C_w \text{ at } y=0, \tag{5}$$

$$u\to 0,\ T\to T_\infty,\ C\to C_\infty \text{ when } y\to\infty. \tag{6}$$

Here the following notation applies: kinematic viscosity $\upsilon\left(=\dfrac{\mu}{\rho_f}\right)$, fluid density ρ_f, dynamic viscosity μ, relaxation time λ_1, electrical conductivity σ, inertia coefficient of a porous medium $F=\dfrac{C_b}{xK^{1/2}}$, gravitational acceleration g, magnetic field strength B_0, thermal expansion coefficient β_t, solutal relaxation time coefficient λ_c, porous medium permeability K, thermal diffusivity $\alpha = \dfrac{k}{(\rho c)_f}$, concentration expansion coefficient β_c, heat capacity ratio $\tau = \dfrac{(\rho c)_p}{(\rho c)_f}$, through liquid heat capacity $(\rho c)_f$, thermophoresis diffusion coefficient D_T, thermal conductivity k, nanoparticle heat capacity $(\rho c)_p$, heat absorption/generation coefficient Q_0, Brownian diffusion coefficient D_B, thermal relaxation time coefficient λ_t, temperature ambient liquid T_∞, liquid concentration C, stretching velocity $u_w(x)$, liquid temperature T, stretching rate c, concentration ambient liquid C_∞, and u, v are the components of velocity in the (x, y) direction respectively.

Introducing the following similarity transformations [64]:

$$\eta = y\sqrt{\frac{c}{\upsilon}}, \theta(\eta) = \frac{T - T_\infty}{T_w - T_\infty}, u = cxf'(\eta), v = -\sqrt{c\upsilon}\, f(\eta), \quad \phi(\eta) = \frac{C - C_\infty}{C_w - C_\infty}. \tag{7}$$

Eq. (1) is justified instinctively, while Eqs. $(2)-(6)$ yield:

$$f''' + ff'' - Ha^2\left(f' - \beta ff''\right) - (1 + F_r)\, f'^2 + \lambda_1(\theta + N\phi) + \beta\left(2ff'f'' - f^2 f'''\right) - \lambda f' = 0, \tag{8}$$

$$\begin{aligned} &\theta'' + \Pr\left(f\theta' + N_b\phi'\theta' + N_t\theta'^2 + S\theta + S\delta_1 f\theta'\right) \\ &+ \Pr\delta_1\left(-ff'\theta' - f^2\theta'' - 2N_t f\theta'\theta'' - N_b f\theta'\phi'' - N_b f\theta''\phi'\right) = 0, \end{aligned} \tag{9}$$

$$\phi'' + Scf\phi' + \frac{N_t}{N_b}\theta'' + Sc\,\delta_2\left(-ff'\phi' - f^2\phi''\right) - \delta_2\frac{N_t}{N_b} f\theta''' = 0, \tag{10}$$

$$f = 0, \theta = 1, \ f' = 1, \ \phi = 1 \text{ at } \eta \to 0, \tag{11}$$

$$\theta \to 0, f' \to 0, \ \phi \to 0 \text{ as } \eta \to \infty. \tag{12}$$

Here $(')$ signifies differentiation with respect to η, Deborah number β, Schmidt number Sc, Fr is Forchheimer inertia coefficient parameter (wherein the quadratic drag coefficient is c_b), Brownian motion parameter N_b, modified Hartmann (magnetohydrodynamic body force) number Ha, Reynolds number Re_x, buoyancy ratio N, Prandtl number $\Pr$, Darcian permeability parameter λ, thermal buoyancy parameter Gr_x, heat absorption variable $S<0$ and heat generation variable $S>0$, (thermal, solutal) relaxation time (δ_1, δ_2). concentration buoyancy parameter Gr^*_x, mixed convection parameter λ_1, thermophoresis variable N_t .

These parameters are defined as follows:

$$\begin{aligned}
&\beta=\lambda a, \lambda=\frac{v}{ka},\ F_r=\frac{c_b}{K^{1/2}},\ Ha^2=\frac{\sigma B_0^2}{a\rho}, \mathrm{Gr}_x\left(=\frac{g\beta_T\left(T_w-T_0\right)x^3}{\upsilon^2}\right),\\
&\mathrm{Gr}_x^*\left(=\frac{g\beta_C\left(C_w-C_0\right)x^3}{\upsilon^2}\right), N=\frac{Gr_x^*}{Gr_x}, \mathrm{Re}_x=\frac{cx^2}{\upsilon}, N_t=\frac{\tau D_T\left(T_f-T_\infty\right)}{T_\infty\upsilon},\\
&\lambda_1=\frac{Gr_x}{\mathrm{Re}_x^2}, \mathrm{Pr}=\frac{\upsilon}{\alpha},\ N_b=\frac{\tau D_B\left(C_f-C_\infty\right)}{\upsilon}, \delta_1=\lambda_t c,\ \delta_2=\lambda_c c,\ S=\frac{Q_0}{\left(\rho c\right)_f c},\\
&Sc=\frac{\upsilon}{D_B}.
\end{aligned} \tag{13}$$

3. **HAM solutions and convergence analysis**

HAM [58] employs an analytical power-series expansion approach which can accommodate many types of linear and nonlinear differential/algebraic equations. The concept of series solutions is also utilized in HAM. Liao [59] was the first who proposed this technique. To solve the transformed ordinary differential equations (8), (9), and (10) along with convective boundary conditions (11-12) using HAM [60-62], the initial guesses $(f_o(\eta), \theta_o(\eta), \phi_o(\eta))$ and supplementary linear functions (L_f, L_θ, L_ϕ) are considered as:

$$\begin{aligned}
f_0(\eta)&=1-e^{-\eta},\\
\theta_0(\eta)&=e^{-\eta},\\
\phi_0(\eta)&=e^{-\eta},
\end{aligned} \tag{14}$$

$$L_\theta=\theta''-\theta,\ L_\phi=\phi''-\phi,\ L_f=f'''-f', \tag{15}$$

with

$$L_f\left(D_1+D_2e^{\eta}+D_3e^{-\eta}\right)=0,\ L_\theta\left(D_4e^{\eta}+D_5e^{-\eta}\right)=0,\ L_\phi\left(D_6e^{\eta}+D_7e^{-\eta}\right)=0, \tag{16}$$

where $D_i\,(i=1-7)$ show the undefined constants.

3.1 Zeroth-order deformation problems

The zeroth order deformation problems are

$$(1-q)L_f\left[\hat{f}(\eta;q)-f_0(\eta)\right]=qh_f N_f[\hat{f}(\eta;q),\hat{\theta}(\eta;q),\hat{\phi}(\eta;q)], \quad \textbf{(17)}$$

$$(1-q)L_\theta\left[\hat{\theta}(\eta;q)-\theta_0(\eta)\right]=qh_\theta N_\theta[\hat{\theta}(\eta;q),\hat{f}(\eta;q),\hat{\phi}(\eta;q)], \quad \textbf{(18)}$$

$$(1-q)L_\phi\left[\hat{\phi}(\eta;q)-\phi_0(\eta)\right]=qh_\phi N_\phi[\hat{\phi}(\eta,q),\hat{f}(\eta,q),\hat{\theta}(\eta;q)], \quad \textbf{(19)}$$

$$\hat{f}(0;q)=0, \quad \hat{f}'(0;q)=1, \quad \hat{f}'(\infty;q)=0 \quad \textbf{(20)}$$

$$\hat{\theta}(0;q)=1,\ \hat{\theta}(\infty;q)=0,\ \hat{\phi}(0;q)=1, \quad \hat{\phi}(\infty;q)=0 \quad \textbf{(21)}$$

$$\begin{aligned}N_f[\hat{f}(\eta,q),\hat{\theta}(\eta;q),\hat{\phi}(\eta;q)]&=\frac{\partial^3\hat{f}(\eta;q)}{\partial\eta^3}+\hat{f}(\eta;q)\frac{\partial^2\hat{f}(\eta;q)}{\partial\eta^2}\\&+\beta\left(2\hat{f}(\eta;q)\frac{\partial\hat{f}(\eta;q)}{\partial\eta}\frac{\partial^2\hat{f}(\eta;q)}{\partial\eta^2}-\left(\hat{f}(\eta;q)\right)^2\frac{\partial^3\hat{f}(\eta;q)}{\partial\eta^3}\right)-\lambda\frac{\partial\hat{f}(\eta;q)}{\partial\eta}\\&-\left(1+F_r\right)\left(\frac{\partial\hat{f}(\eta;q)}{\partial\eta}\right)^2-Ha^2\left(\frac{\partial\hat{f}(\eta;q)}{\partial\eta}-\beta\hat{f}(\eta;q)\frac{\partial^2\hat{f}(\eta;q)}{\partial\eta^2}\right)+\lambda_1\left[\hat{\theta}(\eta;q)+N\hat{\phi}(\eta;q)\right],\end{aligned} \quad \textbf{(22)}$$

$$\begin{aligned}N_\theta[\hat{\theta}(\eta;q),\hat{f}(\eta;q),\hat{\phi}(\eta;q)]&=\frac{\partial^2\hat{\theta}(\eta,q)}{\partial\eta^2}+\Pr\left(\begin{array}{l}\hat{f}(\eta;q)\dfrac{\partial\hat{\theta}(\eta,q)}{\partial\eta}+N_b\dfrac{\partial\hat{\phi}(\eta,q)}{\partial\eta}\dfrac{\partial\hat{\theta}(\eta,q)}{\partial\eta}\\+N_t\left(\dfrac{\partial\hat{\theta}(\eta,q)}{\partial\eta}\right)^2+S\hat{\theta}(\eta;q)+S\delta_1\hat{f}(\eta;q)\dfrac{\partial\hat{\theta}(\eta,q)}{\partial\eta}\end{array}\right)\\&+\Pr\delta_1\left(\begin{array}{l}-\hat{f}(\eta;q)\dfrac{\partial\hat{f}(\eta,q)}{\partial\eta}\dfrac{\partial\hat{\theta}(\eta,q)}{\partial\eta}-\left(\hat{f}(\eta;q)\right)^2\dfrac{\partial^2\hat{\theta}(\eta,q)}{\partial\eta^2}-2N_t\hat{f}(\eta;q)\dfrac{\partial\hat{\theta}(\eta,q)}{\partial\eta}\dfrac{\partial^2\hat{\theta}(\eta,q)}{\partial\eta^2}\\-N_b\hat{f}(\eta;q)\dfrac{\partial\hat{\theta}(\eta,q)}{\partial\eta}\dfrac{\partial^2\hat{\phi}(\eta,q)}{\partial\eta^2}-N_b\hat{f}(\eta;q)\dfrac{\partial^2\hat{\theta}(\eta,q)}{\partial\eta^2}\dfrac{\partial\hat{\phi}(\eta,q)}{\partial\eta}\end{array}\right),\end{aligned} \quad \textbf{(23)}$$

$$\begin{aligned}N_\phi[\hat{\phi}(\eta;q),\hat{f}(\eta;q),\hat{\theta}(\eta;q)]&=\frac{\partial^2\hat{\phi}(\eta,q)}{\partial\eta^2}+\frac{N_t}{N_b}\frac{\partial^2\hat{\theta}(\eta,q)}{\partial\eta^2}+Sc\,\hat{f}(\eta;q)\frac{\partial\hat{\phi}(\eta,q)}{\partial\eta}\\&+Sc\delta_2\left(-\hat{f}(\eta;q)\frac{\partial\hat{f}(\eta,q)}{\partial\eta}\frac{\partial\hat{\phi}(\eta,q)}{\partial\eta}-\left(\hat{f}(\eta;q)\right)^2\frac{\partial^2\hat{\phi}(\eta,q)}{\partial\eta^2}\right)-\delta_2\frac{N_t}{N_b}\hat{f}(\eta;q)\frac{\partial^2\hat{\phi}(\eta,q)}{\partial\eta^2}.\end{aligned} \quad \textbf{(24)}$$

where $q \in [0,1]$ is embedding parameter and h_f , h_θ and h_ϕ are the non-zero auxiliary parameters

3.2 m^th-order deformation problems

$$L_f\left[f_m(\eta) - \chi f_{m-1}(\eta)\right] = h_f R_{f,m}(\eta) \tag{25}$$

$$L_f\left[\theta_m(\eta) - \chi \theta_{m-1}(\eta)\right] = h_\theta R_{\theta,m}(\eta) \tag{26}$$

$$L_\phi\left[\phi_m(\eta) - \chi \phi_{m-1}(\eta)\right] = h_\phi R_{\phi,m}(\eta) \tag{27}$$

$$f_m(0) = 0, \quad f_m'(0) = 0, \quad f_m'(\infty) = 0 \tag{28}$$

$$\theta_m(0) = 0, \; \theta_m(\infty) = 0, \quad \phi_m(0) = 0, \quad \phi_m(\infty) = 0. \tag{29}$$

$$\begin{aligned} \mathrm{R}_m^f(\eta) = {} & f_{m-1}''' + \sum_{k=0}^{m-1}\left(f_{m-1-k} f_k''\right) + \beta \sum_{k=0}^{m-1}\left(2 f_{m-1-k} \sum_{l=0}^{k} f_{k-l}' f_l'' - f_{m-1-k} \sum_{l=0}^{k} f_{k-l} f_l'''\right) \\ & -(1+F_r)\sum_{k=0}^{m-1}\left(f_{m-1-k}' f_k'\right) - Ha^2 f_{m-1}' + Ha^2 \beta \sum_{k=0}^{m-1}\left(f_{m-1-k} f_k''\right) - \lambda f_{m-1}' + \lambda_1\left[\theta_{m-1} + N\phi_{m-1}\right], \end{aligned} \tag{30}$$

$$\begin{aligned} R_m^\theta(\eta) = {} & \theta_{m-1}'' + \Pr \sum_{k=0}^{m-1}\begin{pmatrix} f_{m-1-k}\theta_k' + S\delta_1 f_{m-1-k}\theta_k' \\ +N_b \phi_{m-1-k}'\theta_k' + N_t \theta_{m-1-k}'\theta_k' \end{pmatrix} + \\ & + \Pr \delta_1 \sum_{k=0}^{m-1}\begin{pmatrix} -f_{m-1-k}\sum_{l=0}^{k} f_{k-l}'\theta_l' - f_{m-1-k}\sum_{l=0}^{k} f_{k-l}\theta_l'' - 2N_t f_{m-1-k} \\ \sum_{l=0}^{k}\theta_{k-l}'\theta_l'' - N_b f_{m-1-k}\sum_{l=0}^{k}\theta_{k-l}'\phi_l'' - N_b f_{m-1-k}\sum_{l=0}^{k}\theta_{k-l}''\phi_l' \end{pmatrix}, \end{aligned} \tag{31}$$

$$\begin{aligned} R_m^\phi(\eta) = {} & \phi_{m-1}'' + Sc \sum_{k=0}^{m-1} f_{m-1-k}\phi_k' + \frac{N_t}{N_b}\theta_{m-1}'' + \\ & + Sc\delta_2 \sum_{k=0}^{m-1}\left(f_{m-1-k}\sum_{l=0}^{k} f_{k-l}'\phi_l' - f_{m-1-k}\sum_{l=0}^{k} f_{k-l}\phi''\right) \\ & - \delta_2 \frac{N_t}{N_b}\sum_{k=0}^{m-1} f_{m-1-k}\theta_k''. \end{aligned} \tag{32}$$

$$\chi_m = \begin{cases} 0, & m \le 1 \\ 1, & m > 1 \end{cases} \qquad \textbf{(33)}$$

General solutions are:

$$\begin{cases} F(\eta) = F^*(\eta) + A_1 + A_2 e^{\eta} + A_3 e^{-\eta}, \\ \theta(\eta) = \theta^*(\eta) + A_4 e^{\eta} + A_5 e^{-\eta}, \\ \phi(\eta) = \phi^*(\eta) + A_6 e^{\eta} + A_7 e^{-\eta}, \end{cases} \qquad \textbf{(34)}$$

Here $F^*(\eta)$, $\theta^*(\eta)$ and $\phi^*(\eta)$ are *particular* solutions. The convergence control variables $\hbar_f, \hbar_\theta$ and $\hbar_\phi$ in-series solutions accelerate the convergence of skin friction $f''(0)$, temperature gradient $\theta'(0)$, and nanoparticle concentration gradient $\phi'(0)$. Hence so-called $\hbar$-curves for these variables i.e. $f''(0)$, $\theta'(0)$, $\phi'(0)$ have been depicted in **Figure 2a**. The convergence interval for f, θ and ϕ are $-1.6 \le \hbar_f \le -0.2$, $-1.4 \le \hbar_\theta \le -0.3$ and $-0.9 \le \hbar_\phi \le -0.2$ respectively. The convergent solutions of $f''(0)$, $\theta'(0)$, $\phi'(0)$ are finalized at the 35th order of deformations respectively (see **Table 1**).

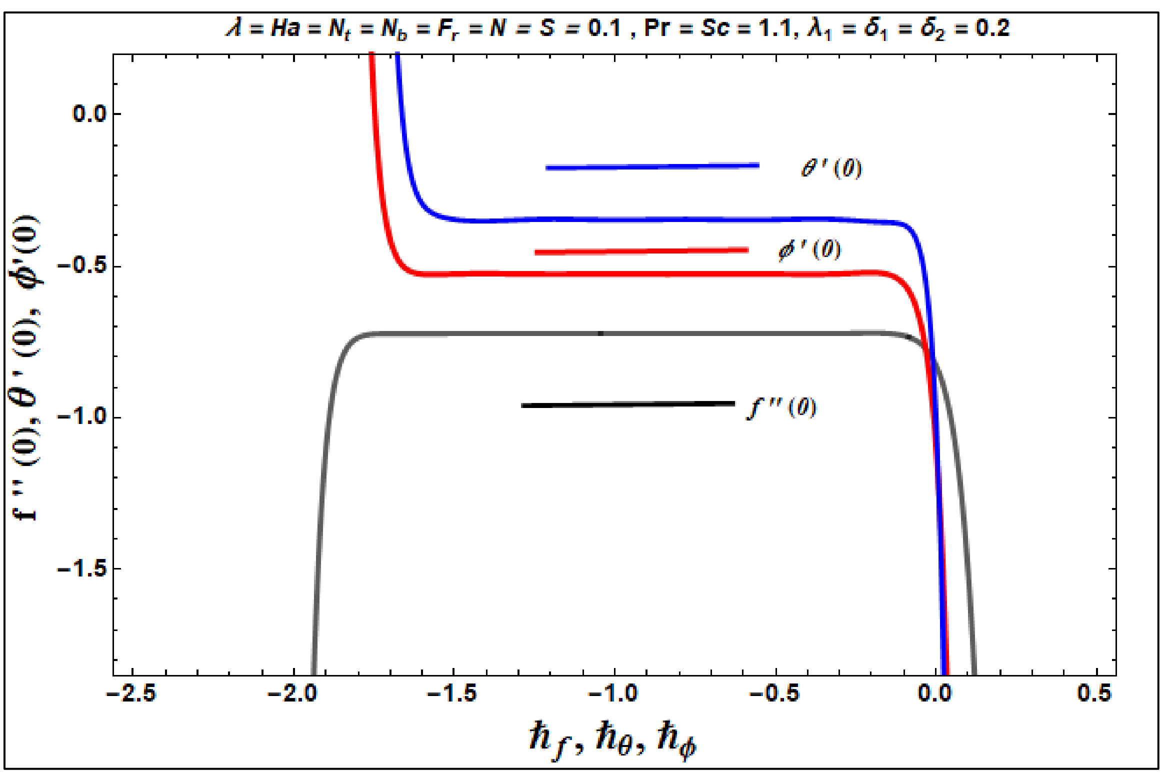

Fig. 2a. $\hbar$–curve impression on $f''(0)$, $\theta'(0)$, $\phi'(0)$ *and* $\chi'(0)$.

Table 1. Convergence series solution of HAM when $\lambda = Ha = F_r = N_t = N_b = S = 0.1,$ $\Pr = Sc = 1.1,\ \beta = \lambda_1 = \delta_1 = \delta_2 = 0.2.$

Order of approximations	$-f''(0)$	$-\theta'(0)$	$-\phi'(0)$
5	0.91565	0.5368	0.3513
10	0.91101	0.5178	0.3549
15	0.91248	0.5242	0.3459
20	0.91291	0.5263	0.3429
25	0.91272	0.5254	0.3450
30	0.91259	0.5248	0.3466
35	0.91262	0.5250	0.3458
40	0.91262	0.5250	0.3458
45	0.91262	0.5250	0.3458

4.Code validation of HAM

Tables 2-4 show comparison results of HAM for verification with other previous simulations. The solutions are compared with Turkyilmazoglu [63], Sadiq and Hayat [64], Hayat *et al*. [65], Irfan *et al.* [66], and Khan *et al.* [67]. The analytical results of skin friction $-C_{fx}\,\mathrm{Re}_x^{-\frac{1}{2}}$ are in very good agreement over a wide range of different parameter variations. Confidence in the present Mathematica-based HAM code is thus validly very higher.

Table 2. Comparison of $-C_{fx}\,\mathrm{Re}_x^{-\frac{1}{2}}$ with Turkyilmazoglu [63] and Sadiq and Hayat [64] for various values of λ.

λ	Turkyilmazoglu [63]	Sadiq and Hayat [64]	Present study
0.0	-1.0000	-1.0000	-1.0000
0.5	-1.22474487	-1.01980	-1.2247
1.0	-1.41421356	-1.11803	-1.4142

Table 3. Comparison of $-C_{fx}\,\mathrm{Re}_x^{-\frac{1}{2}}$ with Sadiq and Hayat [64], and Hayat *et al*. [65] for various values of Ha.

Ha	Hayat *et al.* [65]	Sadiq and Hayat [64]	Present study
0.0	-1.00000	-1.00000	-1.00000
0.2	-1.01980	-1.01980	-1.01980
0.5	-1.11803	-1.11803	-1.11803
0.8	-1.28063	-1.28063	-1.28062
1.0	-1.41421	-1.41421	-1.41421
1.2	-1.56205	-1.56205	-1.56205
1.5	-1.80278	-1.80278	-1.80278

Table 4. Comparison of $-C_{fx}\,\mathrm{Re}_x^{-\frac{1}{2}}$ with Irfan *et al.* [66] and Khan *et al.* [67] for different values of β.

β	Irfan *et al.* [66]	Khan *et al.* [67] (bvp4c)	Khan *et al.* [67] (HAM)	Present study (HAM)
0.0	-1.0000	-1.0000	-1.0000	-1.0000
0.1	-1.02618	-1.02618	-1.02618	-1.02618
0.2	-1.0519	-1.0519	-1.0519	-1.0519
0.3	-1.07712	-1.07712	-1.07712	-1.07712
0.4	-1.1019	-1.1019	-1.1019	-1.1019
0.5	-1.12623	-1.12623	-1.12623	-1.12623
0.6	-1.1501	-1.1501	-1.1501	-1.1501
0.7	-1.17362	-1.17362	-1.17362	-1.17362
0.8	-1.1967	-1.1967	-1.1967	-1.1967
0.9	-1.21941	-1.21941	-1.21941	-1.21941
1.0	-1.24175	-1.24175	-1.24175	-1.24175

5.Results and discussion

In this section, extensive visualization of homotopy method solutions computed in the Mathematica symbolic software is presented. The influence of key physical parameters i.e. Deborah number (Maxwell fluid parameter) β, buoyancy ratio parameter N, Schmidt number Sc, mixed convection parameter λ_1, thermophoresis parameter N_t, heat generation/absorption parameter S, inertia coefficient parameter F_r, Hartmann number Ha, Darcian permeability (porous medium) parameter λ, Prandtl number $\Pr$, solutal relaxation parameter δ_2, Brownian motion diffusion parameter N_b, thermal relaxation parameter δ_1 on velocity $f'(\eta)$, temperature $\theta(\eta)$, nanoparticle concentration $\phi(\eta)$, skin friction $-C_{fx}\,\mathrm{Re}_x^{-\frac{1}{2}}$ is depicted in **Figs. 3a-6e**. Unless otherwise mentioned, the default parameter values $\lambda = Ha = F_r = N_t = N_b = S = 0.1,$ $\Pr = Sc = 1.1,$ $\beta = \lambda_1 = \delta_1 = \delta_2 = 0.2.$ are presumed. This data is consistent with actual nanomaterials deployed in materials processing [68]. It is also verified by scrutiny of earlier studies e.g. [44, 46, 50].

5.1 Velocity distributions

5.1-1 Influence of Deborah number

Fig. 3a. exhibits the characteristics of Deborah (Maxwell fluid) number β against velocity distribution $f'(\eta)$. with greater values of Deborah number β, there is an increment in the velocity $f'(\eta)$. The term Deborah number β arises in the hydrodynamic boundary layer equation (8) with mixed derivative i.e., $\beta\left(2ff'f''-f^2f'''\right)-Ha^2\left(f'-\beta ff''\right)$. The Deborah number shows the ratio between the flow time scale and the relaxation time. In the case of viscoelastic materials, the fluid relaxation parameter is also called the Maxwell parameter. Smaller values of the Maxwell parameter represent Newtonian and viscous fluid behavior, while greater values emphasize non-Newtonian elastic fluid features. Thus, improvement in the Deborah number β, fluid velocity $f'(\eta)$ is observed and strong acceleration is induced via the upsurge in elastic forces relative to viscous forces in the boundary-layer. Momentum boundary-layer thickness therefore decays.

5.1-2 Influence of Forchheimer number

Figure 3b. displays the impact of the Forchheimer number (local inertial force) F_r on velocity $f'(\eta)$. It is found that a reduction in velocity $f'(\eta)$ is witnessed for an enhancement in F_r. The local inertial force has an inverse relation with porous medium permeability, therefore as the inertial force increases. Furthermore, the Forchheimer quadratic drag is accentuated implying that inertial drag effects suppress momentum diffusion. This impedes the percolation of magnetized viscoelastic nanofluid in the porous medium and decelerates the flow. Momentum boundary-layer thickness is augmented. The strong damping effect induced by quadratic drag therefore in not trivial and justifies the inclusion of a non-Darcy formulation. Earlier models have generally neglected this effect and have focused on viscous-dominated low Reynolds number transport for which the Darcian drag component is sufficient. However, the neglection of Forchheimer effects implies that Darcian models over-predict the damping effect on the boundary layer flow. This can have implications for coating quality and deposition rates of nanomaterials. A non-Darcy formulation therefore provides a more comprehensive framework for analyzing transport in sheet stretching nanomaterials fabrication flows.

5.1-3 Influence of Hartmann number

Fig. 3c. reveals the strong retarding influence on the velocity profile $f'(\eta)$ with increment in Hartmann number Ha values. It is obvious that increasing magnetic field accentuates the transverse Lorentzian force which diminishes velocity magnitudes $f'(\eta)$ and increases momentum (hydrodynamic) boundary layer thickness decrease for higher Ha. The strong damping effect of a transverse static magnetic field therefore offers an excellent and non-intrusive mechanism for manipulating momentum characteristics. Flow reversal however is not induced since magnitudes are consistently positive for the velocity field. Asymptotically smooth profiles are achieved at all Hartmann number in the freestream verifying the prescription of a sufficiently larger boundary condition at infinity in the Mathematica HAM code.

5.1-4 Influence of Darcian number

The impact of the Darcian permeability (porous medium) parameter λ on velocity profile $f'(\eta)$ is portrayed in **Fig. 3d.** When this parameter is elevated, a declining trend is observed since the Darcian drag is escalated as the permeability is reduced. The presence of more solid fibers in the porous medium offers greater resistance to the percolating nanofluid at lower permeability values. This damps the velocity field and enhances momentum boundary layer thickness. Again, the selection of appropriate porous filtration media for the stretching sheet regime provides a powerful mechanism for regulating the flow. The magnetic field and porous medium do not interfere in this regard and either or both are useful approaches becoming increasingly popular in nanomaterials fabrication [68].

5.1-5 Influence of mixed convection parameter

Fig. 3e. delineates the effect of mixed convection parameter λ_1 on the velocity $f'(\eta)$. The velocity of the fluid $f'(\eta)$ rises substantially with increasing the values mixed convection parameter λ_1. It is attributable to the accentuation in thermal buoyancy effect with greater values mixed convection parameter λ_1. This mobilizes an intensification in thermal convection currents which accelerate the flow strongly. The momentum (hydrodynamic) boundary layer is depleted with stronger thermal buoyancy.

5.1-6 Influence of buoyancy parameter

Fig. 3f shows the impact of the buoyancy ratio parameter, i. e., $N=\left(\beta_T\left(T-T_\infty\right)+\beta_C\left(C-C_\infty\right)\right)$ on velocity evolution. The relative contribution of solutal buoyancy force to thermal buoyancy force is defined by the (buoyancy ratio parameter) N. It is found that velocity $f'(\eta)$ is higher for greater N since the momentum development is assisted with buoyancy effects. Momentum boundary layer thickness however is reduced. The sturdiest reformation is at intermediary distance from the vertical sheet (wall). At the wall and in the free-stream a weaker influence is computed. The delicate interplay between solutal and thermal buoyancy forces is clearly important in controlling the velocity behaviour. When $N >> 1$, solutal buoyancy strongly dominates the velocity evolution. For $N = 1$ the solutal and thermal buoyancy contribute equally. This leads to strong deceleration. The molecular diffusivity of nanoparticles is instrumental in manipulating the solutal buoyancy force. Materials designers therefore can select appropriate nanoparticles to manipulate the momentum development in the stretching sheet regime.

5.2 Temperature distributions

5.2-1 Influence of Prandtl parameter

Impact of selected parameters on temperature distributions are depicted in **Figs. 4a-4e**. The impact of the Prandtl number $\Pr$ on temperature distribution $\theta(\eta)$ is depicted in **Fig. 4a**. It is observed that here temperature $\theta(\eta)$ decreases with increment in Prandtl number $\Pr$. The Prandtl number $\Pr$ has an opposite relationship with thermal diffusivity, indicating that increasing the Prandtl number causes a decrease in thermal diffusivity i. e. heat diffuses at a slower rate relative to momentum. This cools the regime and depletes fluid temperature $\theta(\eta)$ and thermal boundary layer thickness. The presence of metallic nanoparticles significantly reduces the Prandtl number, and therefore values less than 2 have been studied. Prandtl number is also contrariwise proportional to thermal conductivity. Since nanoparticles increase thermal conductivity significantly, much lower Prandtl numbers are investigated in the plot.

5.2-2 Influence of nanoscale parameters

Figs. 4b and 4c depict the effects of the Buongiorno nanoscale parameters i. e. thermophoresis factor N_t and Brownian motion factor N_b, on temperature $\theta(\eta)$. Here the temperature profile $\theta(\eta)$ and thermal boundary-layer thickness are both elevated with both parameters increasing. Physically, the migration of nanoparticles is intensified under thermal gradient (thermophoresis, N_t) into the boundary layer. This heats the regime and boosts temperature profile $\theta(\eta)$. Heat transportation from wall to the boundary-layer is amplified for the non-Newtonian nanofluid. With increasing Brownian motion parameter N_b, ballistic collisions between nanoparticles are exacerbated in the regime. This generates heat generation via transfiguration of kinetic energy into thermal energy. Micro-convection around the nanoparticles will also be boosted. Thermal boundary-layer thickness is therefore increased.

5.2-3 Influence of non-Fourier thermal relaxation parameter

Fig.4d portrays the influence of the (non-Fourier thermal relaxation parameter) δ_1 on temperature distribution $\theta(\eta)$. One can notice that fluid temperature $\theta(\eta)$ and thickness of the thermal boundary-layer are decreased through higher δ_1 . With stronger thermal relaxation, the temperature is reduced since there is a delay in heat transfer to nanofluid molecules. Alternatively, by fixing $\delta_1 = 0$, for the classical Fourier model, heat is distributed instantaneously throughout the nanofluid. This approach therefore produces higher temperatures and a greater thermal boundary-layer thickness, and essentially over-predicts the temperature distribution. The revised Cattaneo–Christov **(**non-Fourier**)** heat flux theory, *avoids this over-prediction* and also achieves a more appropriate estimate of thermal boundary-layer thickness. The cooling effect with thermal relaxation is properly captured with the non-Fourier law and materials designers can therefore achieve a more precise appraisal of the thermophysics [68].

5.2-4 Influence of heat source/sink parameter

Fig. 4e represents the effect of heat generation/absorption factor S on dimensionless temperature $\theta(\eta)$. The thermal boundary-layer Eqn. (9) contains two terms viz, ($+S\theta + S\delta_1 f\theta'$) for this parameter S . These are non-Fourier and classical Fourier terms, respectively. The **(**non-Fourier**)** thermal relaxation time δ_1 is featured in this latter. It is evident that with positive enhancement in S (heat generation $S > 0$), the temperature profile $\theta(\eta)$ decreased dramatically and thermal boundary-layer thickness is reduced. However, the differing scenario is observed for enhancement in negative S (thermal absorption $S < 0$) which actually elevates temperatures and thermal boundary-layer thickness. The non-Fourier behaviour therefore produces a very different overall influence of thermal generation (and sink) compared with classical Fourier approaches.

5.3 Nanoparticle concentration profiles

Figs 5a-5d show the development in nanoparticle concentration profiles with selected parameters.

5.3-1 Influence of Schmidt number

Fig. 5a demonstrates the variations in nanoparticle concentration $\phi(\eta)$ for several values of Schmidt number Sc . It is known that Schmidt number defines the ratio of viscosity to molecular (nanoparticle species) diffusivity ratio. A strong intensification in Schmidt number, therefore, corresponds to a decrement in mass diffusivity i. e. the diffusion rate of nanoparticles relative to momentum diffusion is suppressed. As a result, the nanoparticle concentration $\phi(\eta)$ and thickness of the concentration boundary layer are reduced. Again, the selection of appropriate nanoparticles is critical in manipulating mass transfer characteristics.

5.3-2 Influence of nanoscale parameters

Figs. 5b and 5c demonstrate the collective impact of the nanoscale parameters i.e. Brownian motion diffusion parameter N_b and thermophoresis parameter N_t on nanoparticle concentrations $\phi(\eta)$. A stronger thermophoresis effect results in a boost, whereas greater Brownian motion results in a decrement. In opposite to species diffusion, the enhanced ballistic collisions of nanoparticles with stronger Brownian motion inhibits the spread of nanoparticles and manifests in a thinner concentration boundary layer thickness. However, as the (thermophoretic body force) effect increases (higher N_t) stimulates the movement of nanoparticles in the boundary layer from hotter to colder areas under the driving temperature gradient. This enhances the concentration of nanoparticles, resulting in a stronger concentration boundary layer.

5.3-3 Influence of non-Fickian solutal relaxation parameter

The influence of non-Fickian solutal relaxation parameter, δ_2 on concentration, $\phi(\eta)$ is demonstrated in **Fig. 5d.** Higher values of the (non-Fickian**)** solutal relaxation parameter result in a lower concentration profile. The solutal relaxation effect delays the diffusion of nanoparticle species. This also decreases the thickness of the nanoparticle solutal boundary layer. Again, for the Fickian case nanoparticle concentrations will be over-estimated since the relaxation effect is ignored (δ_2 = 0).

5.4 Skin friction distributions

Figs. 6a–6e display the impact of the Maxwell rheological viscoelastic parameter β, inertia coefficient parameter F_r, Hartman number Ha, Darcian permeability parameter λ and the buoyancy ratio parameter N) on skin friction $-C_{fx}\,\mathrm{Re}_x^{-\frac{1}{2}}$ versus mixed convection parameter λ_1 . It is evident that an augmentation in the (Hartmann number Ha, inertia coefficient F_r, and Darcian parameter, λ parameters) yields a stronger intensification in the skin friction $-C_{fx}\,\mathrm{Re}_x^{-\frac{1}{2}}$ magnitude as shown in figs. 6b-6d. However, in these graphs, the profiles decrease linearly as the dual (mixed) convection variable λ_1 increases. On the other hand, there is an extensive reduction reported in $-C_{fx}\,\mathrm{Re}_x^{-\frac{1}{2}}$ with enhancement in (Maxwell liquid parameter β and buoyancy ratio factor N - see Fig 6e). Both figures again show a linear decay of the profiles as the mixed convection variable λ_1 increases.

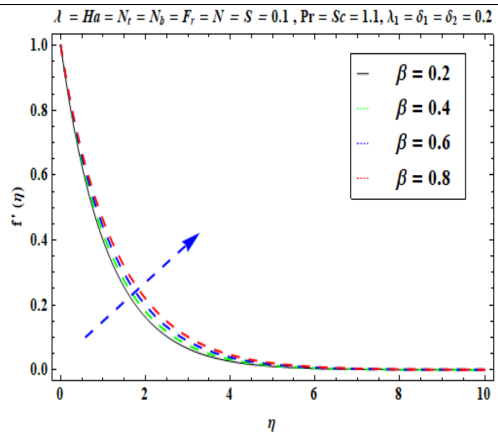

Fig. 3a. $f'(\eta)$ against β.

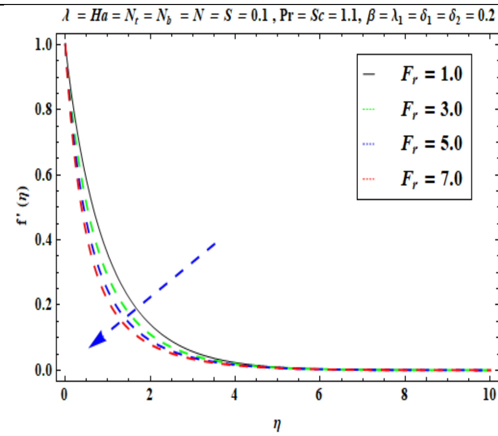

Fig. 3b. $f'(\eta)$ against F_r.

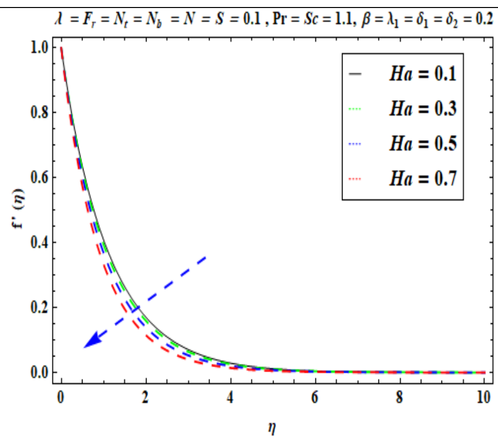

Fig. 3c. $f'(\eta)$ against Ha.

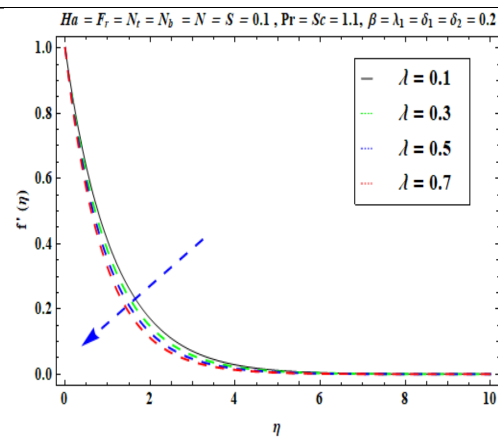

Fig. 3d. $f'(\eta)$ against λ.

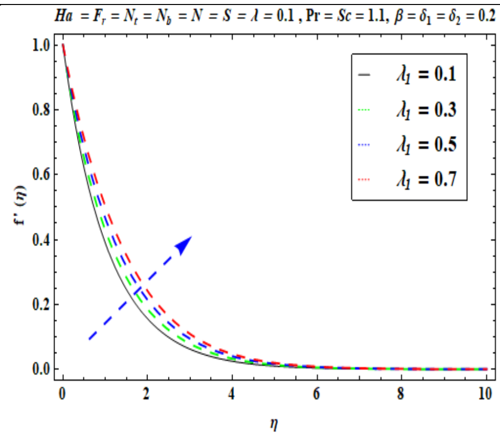

Fig. 3e. $f'(\eta)$ against λ_1.

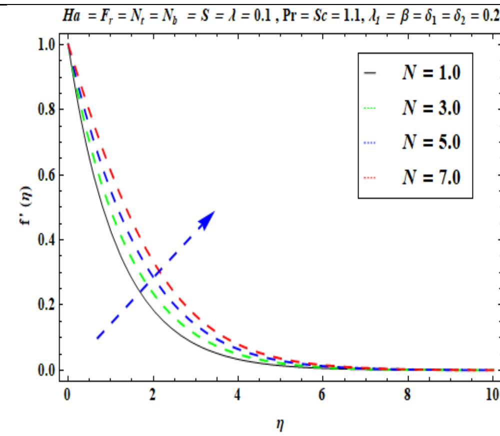

Fig. 3f. $f'(\eta)$ against N.

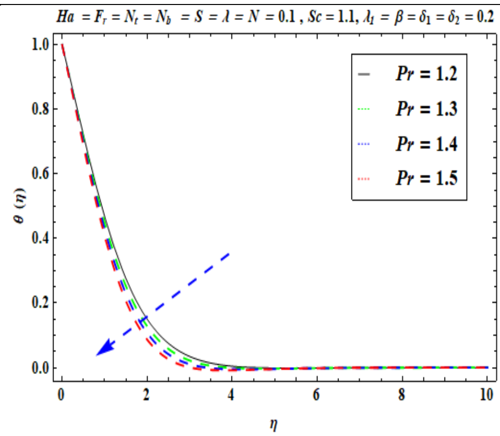

Fig. 4a. $\theta(\eta)$ against $\Pr$.

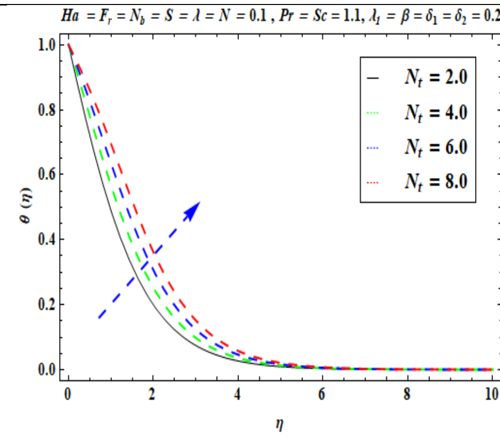

Fig. 4b. $\theta(\eta)$ against N_t.

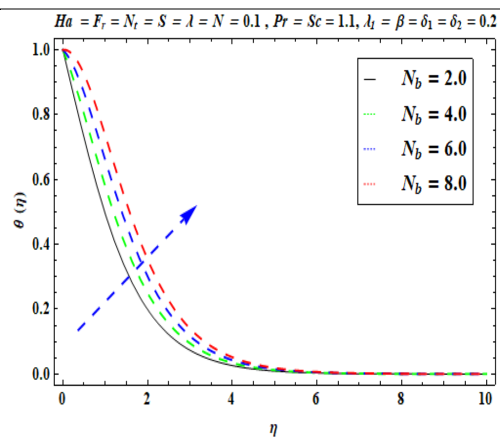

Fig. 4c. $\theta(\eta)$ against N_b.

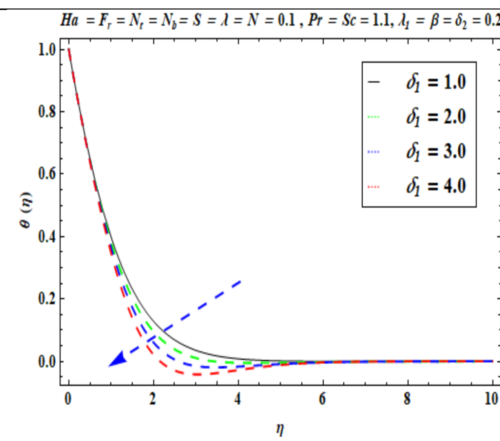

Fig. 4d. $\theta(\eta)$ against δ_1.

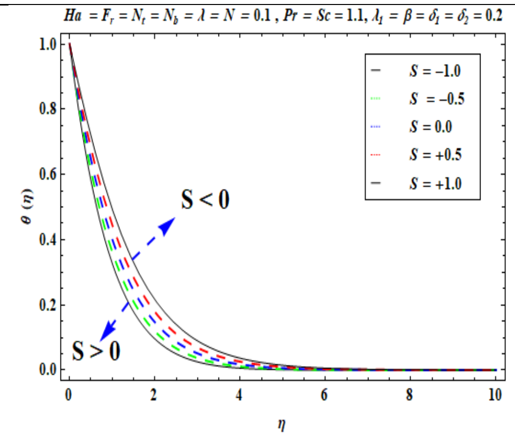

Fig. 4e. $\theta(\eta)$ against S.

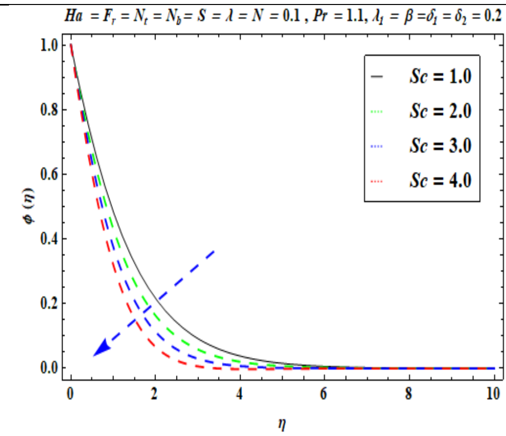

Fig. 5a. $\phi(\eta)$ against Sc.

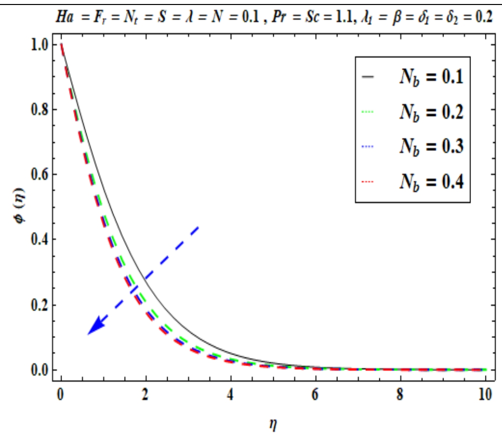

Fig. 5b. $\phi(\eta)$ against N_b.

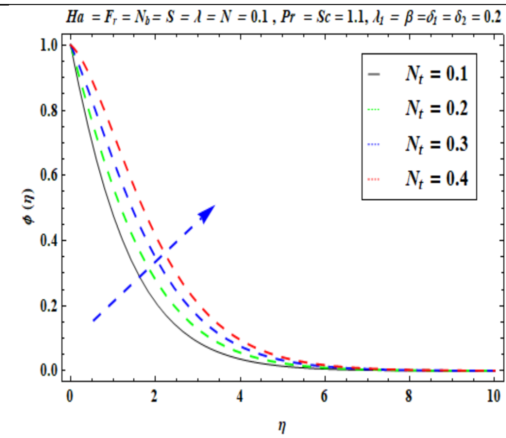

Fig. 5c. $\phi(\eta)$ against N_t.

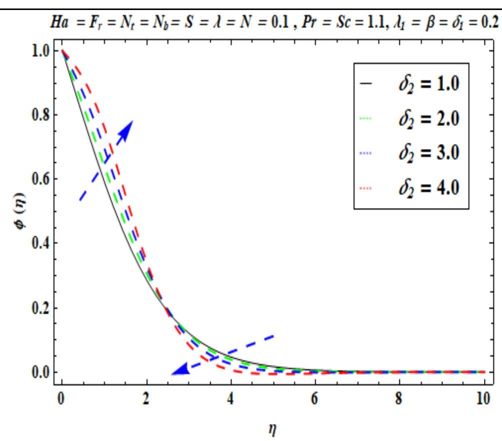

Fig. 5d. $\phi(\eta)$ against δ_2.

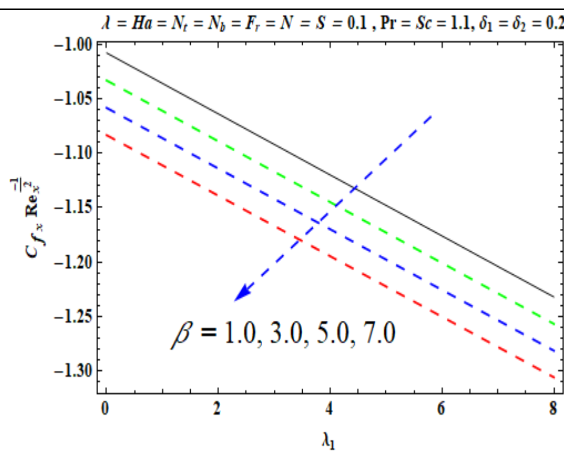

Fig. 6a. $Cf_x \, Re_x^{\frac{-1}{2}}$ against β.

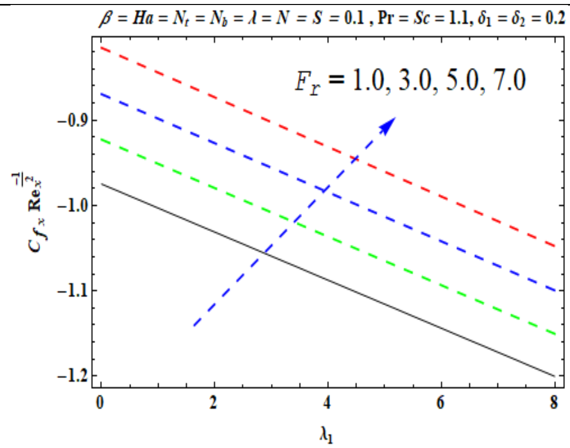

Fig. 6b. $Cf_x \mathrm{Re}_x^{\frac{-1}{2}}$ against F_r.

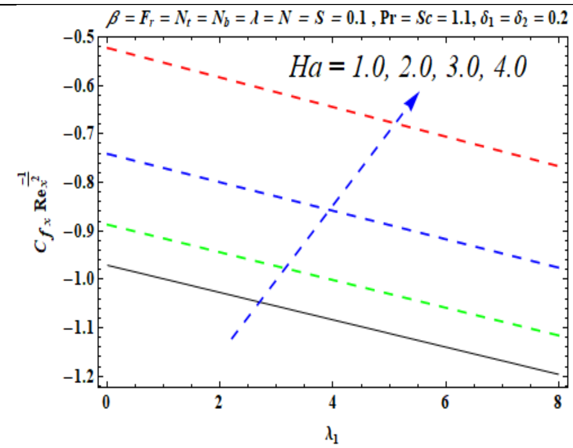

Fig. 6c. $Cf_x \mathrm{Re}_x^{\frac{-1}{2}}$ against Ha.

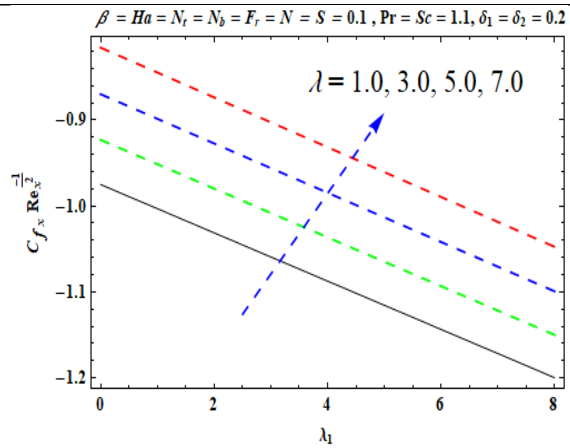

Fig. 6d. $Cf_x \mathrm{Re}_x^{\frac{-1}{2}}$ against λ.

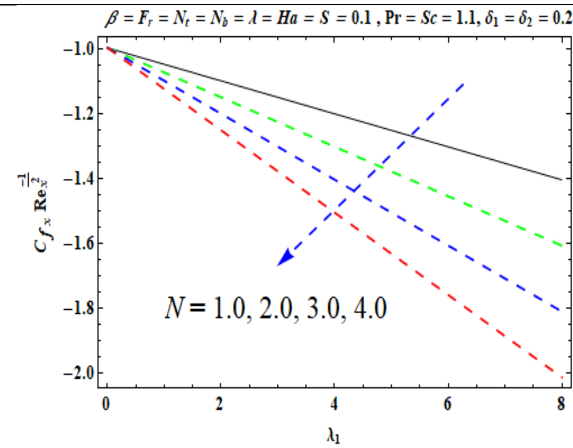

Fig. 6e. $Cf_x \mathrm{Re}_x^{\frac{-1}{2}}$ against N.

6.Conclusions

Motivated by simulating more realistically magnetohydrodynamic nanomaterials manufacturing processes, a mathematical model has been established for non-*Fourier and non-Fickian electro-conductive mixed convection thermo-solutal Maxwell viscoelastic nanopolymer flow induced by stretching vertical surface adjacent to a non-Darcian porous medium.* Buongiorno's nanofluid model has been to simulate the nanoscale effects of Brownian motion diffusion and thermophoresis. Heat generation/absorption effects have also been included. For the porous medium, which is anticipated to be isotropic and homogenous, the Darcy-Forchheimer drag force model has been deployed. To scale the non-similar flow problem, appropriate transformations are and the primitive partial differential equation boundary value problem is reformulated as a nonlinear ordinary differential one. The dimensionless sets of nonlinear differential equations with associated wall and free stream boundary conditions are then solved with the power-series expansion approach in the homotopy analysis methodology (HAM). Numerical evaluation of series solutions is conducted in Mathematica software. A thorough parametric investigation is carried out to elucidate the characteristics of key control variables on velocity $f'(\eta)$, temperature $\theta(\eta)$, nanoparticle concentration $\phi(\eta)$ and skin friction $-C_{fx}\,\mathrm{Re}_x^{-\frac{1}{2}}$. Comparison results of HAM for the authentication of analytical technique with the literature is also included and a convergence study is furthermore included. The findings of this study can be described consequently:

(i) An increasing trend is witnessed in velocity $f'(\eta)$ and momentum boundary-layer thickness with greater estimations of Maxwell non-Newtonian material parameter β and mixed convection parameter λ_1.

(ii) Temperature $\theta(\eta)$ is strongly reduced with increment in non-Fourier thermal relaxation variable δ_1 and Prandtl number Pr. The classical Fourier model (δ_1=0) which is parabolic is shown to over-predict temperature and thermal boundary-layer thickness indicating that it is inaccurate for realistic nanomaterials manufacturing processes.

(iii) A stronger (heat absorption variable $S<0$) boosts temperature magnitudes whereas an enhancement in the (heat generation variable $S>0$) diminishes temperature and also reduces the thermal boundary-layer thickness.

(iv) The concentration of nanoparticles $\phi(\eta)$ and temperature $\theta(\eta)$ are both decreasing functions of the thermal relaxation variable δ_1 and solutal δ_2 relaxation variable.

(v) The concentration of nanoparticles $\phi(\eta)$ exhibits an opposite trend with increment in Brownian movement diffusion parameter N_b and thermophoretic N_t variable.

(vi) Concentration along with boundary-layer thickness decrease with increasing estimations of Schmidt number Sc, and this is related to the decrease in molecular diffusivity of nanoparticles.

(vii) Elevations in Hartmann (magnetic) number Ha, Darcian permeability parameter λ, and Forchheimer inertia coefficient parameter F_r all increase the skin friction coefficients

$-C_{fx}\,\mathrm{Re}_x^{-\frac{1}{2}}$. However, the contrary behaviour is computed with an increment in Maxwell fluid variable β along with buoyancy ratio variable N.

(viii) HAM has been shown to be an exceptionally accurate semi-numerical technique which achieves faster convergence and excellent accuracy and is very suitable for nonlinear multi-physical transport problems in nano-materials processing.

Overall, the current study has demonstrated that non-Fourier and non-Fickian models in conjunction with nonlinear rheological (viscoelastic) nanofluid behaviour are important in more realistically simulating nanomaterial coating flow characteristics in stretching sheet manufacturing processes. Future studies may consider chemical reaction along with activation energy aspects under revised Fourier and revised Fickian's theory and also examine hybrid nanofluids for both stretching and shrinking surfaces [69].

References

1]. Cattaneo, C. (1948). Sulla conduzione del calore. *Atti Sem. Mat. Fis. Univ. Modena*, *3*, 83-101.

2]. Christov, C. I. (2009). On frame indifferent formulation of the Maxwell–Cattaneo model of finite-speed heat conduction. *Mechanics Research Communications*, *36*(4), 481-486.

3]. Ijaz, M., Yousaf, M., & El Shafey, A. M. (2021). Arrhenius activation energy and Joule heating for Walter-B fluid with Cattaneo–Christov double-diffusion model. *Journal of Thermal Analysis and Calorimetry*, *143*(5), 3687-3698.

4]. Hafeez, A., Khan, M., Ahmed, A., & Ahmed, J. (2021). Features of Cattaneo-Christov double diffusion theory on the flow of non-Newtonian Oldroyd-B nanofluid with Joule heating. *Applied Nanoscience*, 1-8.

5]. Rawat, S. K., Upreti, H., & Kumar, M. (2021). Numerical study of activation energy and thermal radiation effects on Oldroyd-B nanofluid flow using the Cattaneo–Christov double diffusion model over a convectively heated stretching sheet. *Heat Transfer*, *50*(6), 5304-5331.

6]. Haider, A., Ayub, A., Madassar, N., Ali, R. K., Sabir, Z., Shah, S. Z., & Kazmi, S. H. (2021). Energy transference in time-dependent Cattaneo–Christov double diffusion of second-grade fluid with variable thermal conductivity. *Heat Transfer*, *50*(8), 8224-8242.

7]. Chu, Y. M., Shankaralingappa, B. M., Gireesha, B. J., Alzahrani, F., Khan, M. I., & Khan, S. U. (2022). Combined impact of Cattaneo-Christov double diffusion and radiative heat flux on bio-convective flow of Maxwell liquid configured by a stretched nano-material surface. *Applied Mathematics and Computation*, *419*, 126883.

8]. Khan, S. A., Waqas, H., Naqvi, S. M. R. S., Alghamdi, M., & Al-Mdallal, Q. (2021). Cattaneo-Christov double diffusions theories with bio-convection in nanofluid flow to enhance the efficiency of nanoparticles diffusion. *Case Studies in Thermal Engineering*, *26*, 101017.

9]. Ibrahim, W., & Gadisa, G. (2020). Finite element solution of nonlinear convective flow of Oldroyd-B fluid with Cattaneo-Christov heat flux model over nonlinear stretching sheet with heat generation or absorption. *Propulsion and Power Research*, *9*(3), 304-315.

10]. Khan, M. I., Alzahrani, F., Hobiny, A., & Ali, Z. (2020). Modeling of Cattaneo-Christov double diffusions (CCDD) in Williamson nanomaterial slip flow subject to porous medium. *Journal of Materials Research and Technology*, *9*(3), 6172-6177.

11]. Crane, L. J. (1970). Flow past a stretching plate. *Zeitschrift für angewandte Mathematik und Physik ZAMP*, *21*(4), 645-647.

12]. Jafarimoghaddam, A. (2018). Two-phase modeling of three-dimensional MHD porous flow of Upper-Convected Maxwell (UCM) nanofluids due to a bidirectional stretching surface: Homotopy perturbation method and highly nonlinear system of coupled equations. *Engineering science and technology, an international journal*, *21*(4), 714-726.

13]. Habib, U., Abdal, S., Siddique, I., & Ali, R. (2021). A comparative study on micropolar, Williamson, Maxwell nanofluids flow due to a stretching surface in the presence of bioconvection, double diffusion and activation energy. *International Communications in Heat and Mass Transfer*, *127*, 105551.

14]. Prasannakumara, B. C. (2021). Numerical simulation of heat transport in Maxwell nanofluid flow over a stretching sheet considering magnetic dipole effect. *Partial Differential Equations in Applied Mathematics*, *4*, 100064.

15]. Daoud, Y., Abdalbagi, M., & Khidir, A. A. (2021). On the solution of magneto-hydrodynamics three-dimensional flow due to a stretching sheet in a porous medium using the successive linearization method. *Chinese Journal of Physics*, *73*, 232-238.

16]. Kumar, R. N., Jyothi, A. M., Alhumade, H., Gowda, R. P., Alam, M. M., Ahmad, I., ... & Prasannakumara, B. C. (2021). Impact of magnetic dipole on thermophoretic particle deposition in the flow of Maxwell fluid over a stretching sheet. *Journal of Molecular Liquids*, *334*, 116494.

17]. Hsiao, K. L. (2017). Combined electrical MHD heat transfer thermal extrusion system using Maxwell fluid with radiative and viscous dissipation effects. *Applied Thermal Engineering*, *112*, 1281-1288.

18]. Seid, E., Haile, E., & Walelign, T. (2022). Multiple slip, Soret and Dufour effects in fluid flow near a vertical stretching sheet in the presence of magnetic nanoparticles. *International Journal of Thermofluids*, *13*, 100136.

19]. Mahabaleshwar, U. S., Sneha, K. N., & Huang, H. N. (2021). An effect of MHD and radiation on CNTS-Water based nanofluids due to a stretching sheet in a Newtonian fluid. *Case Studies in Thermal Engineering*, *28*, 101462.

20]. Imtiaz, M., Mabood, F., Hayat, T., & Alsaedi, A. (2021). Impact of non-Fourier heat flux in bidirectional flow of carbon nanotubes over a stretching sheet with variable thickness. *Chinese Journal of Physics*.

21]. Awati, V. B., Kumar, M., & Wakif, A. (2021). Haar wavelet scrutinization of heat and mass transfer features during the convective boundary layer flow of a nanofluid moving over a nonlinearly stretching sheet. *Partial Differential Equations in Applied Mathematics*, *4*, 100192.

22]. Ramana, R. M., Raju, K. V., & Kumar, J. G. (2022). Multiple slips and heat source effects on MHD stagnation point flow of casson fluid over a stretching sheet in the presence of chemical reaction. *Materials Today: Proceedings*, *49*, 2306-2315**.**

23]. Choi, S. U., & Eastman, J. A. (1995). *Enhancing thermal conductivity of fluids with nanoparticles* (No. ANL/MSD/CP-84938; CONF-951135-29). Argonne National Lab.(ANL), Argonne, IL (United States).

24]. Eid, M. R., Mahny, K. L., Dar, A., & Muhammad, T. (2020). Numerical study for Carreau nanofluid flow over a convectively heated nonlinear stretching surface with chemically reactive species. *Physica A: Statistical Mechanics and its Applications*, *540*, 123063.

25]. Jamaludin, A., Naganthran, K., Nazar, R., & Pop, I. (2020). MHD mixed convection stagnation-point flow of Cu-Al2O3/water hybrid nanofluid over a permeable stretching/shrinking surface with heat source/sink. *European Journal of Mechanics-B/Fluids*, *84*, 71-80.

26]. Salawu, S. O., Fatunmbi, E. O., & Okoya, S. S. (2021). MHD heat and mass transport of Maxwell Arrhenius kinetic nanofluid flow over stretching surface with nonlinear variable properties. *Results in Chemistry*, *3*, 100125.

27]. Hsiao, K. L. (2016). Stagnation electrical MHD nanofluid mixed convection with slip boundary on a stretching sheet. *Applied Thermal Engineering*, *98*, 850-861.

28]. Hsiao, K. L. (2017). To promote radiation electrical MHD activation energy thermal extrusion manufacturing system efficiency by using Carreau-Nanofluid with parameters control method. *Energy*, *130*, 486-499.

29]. Hsiao, K. L. (2017). Micropolar nanofluid flow with MHD and viscous dissipation effects towards a stretching sheet with multimedia feature. *International Journal of Heat and Mass Transfer*, *112*, 983-990.

30]. Awan, A. U., Shah, S. A. A., & Ali, B. (2022). Bio-convection effects on Williamson nanofluid flow with exponential heat source and motile microorganism over a stretching sheet. *Chinese Journal of Physics*.

31]. Kumbhakar, B., & Nandi, S. (2022). Unsteady MHD radiative-dissipative flow of Cu-Al2O3/H2O hybrid nanofluid past a stretching sheet with slip and convective conditions: A regression analysis. *Mathematics and Computers in Simulation*, *194*, 563-587.

32]. Chu, Y. M., Khan, M. I., Abbas, T., Sidi, M. O., Alharbi, K. A. M., Alqsair, U. F., ... & Malik, M. Y. (2022). Radiative thermal analysis for four types of hybrid nanoparticles subject to non-uniform heat source: Keller box numerical approach. *Case Studies in Thermal Engineering*, *40*, 102474.

33]. Bafakeeh, O. T., Raza, A., Khan, S. U., Khan, M. I., Nasr, A., Khedher, N. B., & Tag-Eldin, E. S. M. (2022). Physical Interpretation of Nanofluid (Copper Oxide and Silver) with Slip and Mixed Convection Effects: Applications of Fractional Derivatives. *Applied Sciences*, *12*(21), 10860.

34]. Zahoor Raja, M. A., Shoaib, M., Tabassum, R., Khan, M. I., Jagannatha, C. G., & Gali, C. (2022). Performance analysis of backpropagated networks for entropy optimized mixed convection nanofluid with second-order slip over a stretching surface. *Waves in Random and Complex Media*, 1-23.

35]. Ahmed, M. F., Zaib, A., Ali, F., Bafakeeh, O. T., Tag-ElDin, E. S. M., Guedri, K., ... & Khan, M. I. (2022). Numerical computation for gyrotactic microorganisms in mhd radiative eyring–powell nanomaterial flow by a static/moving wedge with Darcy–Forchheimer Relation. *Micromachines*, *13*(10), 1768.

36]. Abbasi, A., Farooq, W., Tag-ElDin, E. S. M., Khan, S. U., Khan, M. I., Guedri, K., ... & Galal, A. M. (2022). Heat transport exploration for hybrid nanoparticle (Cu, Fe_3O_4)—based blood flow via tapered complex wavy curved channel with slip features. *Micromachines*, *13*(9), 1415.

37]. Waqas, H., Oreijah, M., Guedri, K., Khan, S. U., Yang, S., Yasmin, S., ... & Galal, A. M. (2022). Gyrotactic motile micro-organisms impact on pseudoplastic nanofluid flow over a moving Riga surface with exponential heat flux. *Crystals*, *12*(9), 1308.

38]. Bafakeeh, O. T., Raghunath, K., Ali, F., Khalid, M., Tag-ElDin, E. S. M., Oreijah, M., ... & Khan, M. I. (2022). Hall Current and Soret Effects on Unsteady MHD Rotating Flow of Second-Grade Fluid through Porous Media under the Influences of Thermal Radiation and Chemical Reactions. *Catalysts*, *12*(10), 1233.

39]. Harshavardhan, A., Matt, S. B., Khan, M. I., Prakash, K. K., Alnuwaiser, M. A., Betageri, V. S., & Sidlinganahalli, M. (2022). Synthesis of Tin oxide nanoparticles using Nelumbo nucifera leaves extract for electrochemical sensing of dopamine. *International Journal of Modern Physics B*, 2350108.

40]. A. A. Pasha, K. Irshad, S. Algarni, T. Alqahtani and M. Waqas, Analysis of tangent-hyperbolic rheological model considering nonlinear mixed convection, Joule heating and Soret-Dufour aspects from a stretchable convective stratified surface, International Communications in Heat and Mass Transfer (2022)

41]. N. Anjum, W. A. Khan, M. Azam, M. Ali, M. Waqas and I. Hussain, Significance of bioconvection analysis for thermally stratified 3D Cross nanofluid flow with gyrotactic microorganisms and activation energy aspects, *Thermal Science and Engineering Progress* (2022)

42]. A. A. Pasha, Z. Hussain, M. M. Alam, N. Kasim, K. Irshad, M. Ali, M. Waqas and W. A. Khan, Impact of magnetized non-linear radiative flow on 3D chemically reactive sutterby nanofluid capturing heat sink/source aspects, *Case Studies in Thermal Engineering* (2022)

43]. Qaiser, D., Zheng, Z., & Khan, M. R. (2021). Numerical assessment of mixed convection flow of Walters-B nanofluid over a stretching surface with Newtonian heating and mass transfer. *Thermal Science and Engineering Progress*, *22*, 100801.

44]. Patil, P. M., Kulkarni, M., & Hiremath, P. S. (2020). Effects of surface roughness on mixed convective nanofluid flow past an exponentially stretching permeable surface. *Chinese Journal of Physics*, *64*, 203-218.

45]. Puneeth, V., Manjunatha, S., Madhukesh, J. K., & Ramesh, G. K. (2021). Three-dimensional mixed convection flow of hybrid casson nanofluid past a non-linear stretching surface: A modified Buongiorno's model aspects. *Chaos, Solitons & Fractals*, *152*, 111428.

46]. Waini, I., Ishak, A., & Pop, I. (2020). Mixed convection flow over an exponentially stretching/shrinking vertical surface in a hybrid nanofluid. *Alexandria Engineering Journal*, *59*(3), 1881-1891.

47]. Rehman, S., Rehman, S. U., Khan, A., & Khan, Z. (2020). The effect of flow distribution on heat and mass transfer of MHD thin liquid film flow over an unsteady stretching sheet in the presence of variational physical properties with mixed convection. *Physica A: Statistical Mechanics and its Applications*, *551*, 124120.

48]. Nasir, M., Waqas, M., Bég, O. A., Basha, D. B., Zamri, N., Leonard, H. J., & Khan, I. (2022). Chemically reactive Maxwell nanoliquid flow by a stretching surface in the frames of Newtonian heating, nonlinear convection and radiative flux: Nanopolymer flow processing simulation. *Nanotechnology Reviews*, *11*(1), 1291-1306.

49]. Nasir, M., Waqas, M., Kausar, M. S., Bég, O. A., & Zamri, N. (2022). Cattaneo-Christov dual diffusive non-Newtonian nanoliquid flow featuring nonlinear convection. *Chinese Journal of Physics*.

50]. Amiril SAS, Rahim EA, Syahrullail S, A review on ionic liquids as sustainable lubricants in manufacturing and engineering: recent research, performance, and applications. *J Clean Prod* 168:1571–1589 (2017).

51]. Biksa A, Yamamoto K, Dosbaeva G, Veldhuis SC, Fox-Rabinovich GS, Elfizy A, Wagg T, Shuster LS (2010) Wear behavior of adaptive nano-multilayered AlTiN/MexN PVD coatings during machining of aerospace alloys. *Tribol Int* 43:1491–149.

52] A.N. Bolotov, V.V. Novikov, O.O. Novikova, Friction of a structured magnetic fluid sliding over a solid surface, *J. of Friction and Wear.* 27(4) (2006) 46–51.

53] A.N. Bolotov, G.B. Burdo, V.V. Novikov, O.O. Novikova, The influence of magnetic field on the structure and properties of nanostructured ferrofluid lubricating oil, *Physical and chemical aspects of studying clusters, nanostructures and nanomaterials*. 7 (2015) 137–141.

54] R. Sahoo et al., Design of smart lubricants using the inverse ferrofluid approach, *Tribology International*, 166 (2022). 107346

55] P. Zhang, K.H. Lee, C.H. Lee, Friction characteristics of magneto-rheological fluid on DLC- and PTFE-coated surfaces, *ASME J Eng Trib*, 231 (2017), pp. 1-9.

56] R. Saldivar-Guerrero, R. Richter, I. Rehberg, N. Aksel, L. Heymann, O.S. Rodriguez-Fernandez, Viscoelasticity of mono- and polydisperse inverse ferrofluids, *J Chem Phys*, 125 (2006), Article 084907.

57] Ashtiani, M., Hashemabadi, S. H., and Ghaffari, A. (2015). A review on the magnetorheological fluid preparation and stabilization. *J. Mag. Mag. Mater*. 374, 716–730.

58] Liao, S. (2003). *Beyond perturbation: introduction to the homotopy analysis method*. Chapman and Hall/CRC.

59] Liao, S. (2012). *Homotopy analysis method in nonlinear differential equations* (pp. 153-165). Beijing: Higher education press.

60] Hayat, T., Khan, M. I., Waqas, M., Yasmeen, T., & Alsaedi, A. (2016). Viscous dissipation effect in flow of magnetonanofluid with variable properties. *Journal of Molecular Liquids*, *222*, 47-54.

61] Hayat, T., Muhammad, T., Shehzad, S. A., & Alsaedi, A. (2017). An analytical solution for magnetohydrodynamic Oldroyd-B nanofluid flow induced by a stretching sheet with heat generation/absorption. *International Journal of Thermal Sciences*, *111*, 274-288.

62] Hayat, T., Abbas, T., Ayub, M., Muhammad, T., & Alsaedi, A. (2016). On squeezed flow of Jeffrey nanofluid between two parallel disks. *Applied Sciences*, *6*(11), 346.

63] Turkyilmazoglu, M. (2013). The analytical solution of mixed convection heat transfer and fluid flow of a MHD viscoelastic fluid over a permeable stretching surface. *International Journal of Mechanical Sciences*, *77*, 263-268.

64] Sadiq, M. A., & Hayat, T. (2016). Darcy–Forchheimer flow of magneto Maxwell liquid bounded by convectively heated sheet. *Results in Physics*, *6*, 884-890.

65] Hayat, T., Khan, M. I., Farooq, M., Alsaedi, A., Waqas, M., & Yasmeen, T. (2016). Impact of Cattaneo–Christov heat flux model in flow of variable thermal conductivity fluid over a variable thicked surface. *International Journal Heat Mass Transfer*, *99*, 702-710.

66] Irfan, M., Khan, M., & Khan, W. A. (2019). Impact of homogeneous–heterogeneous reactions and non-Fourier heat flux theory in Oldroyd-B fluid with variable conductivity. *Journal of the Brazilian Society of Mechanical Sciences and Engineering*, *41*(3), 1-9.

67] Khan, M., Ahmed, A., Irfan, M., & Ahmed, J. (2021). Analysis of Cattaneo–Christov theory for unsteady flow of Maxwell fluid over stretching cylinder. *Journal of Thermal Analysis and Calorimetry*, *144*(1), 145-154.

68] Vajtai, R. (Ed.). (2013). *Springer Handbook of Nanomaterials*. Springer Science & Business Media.

69] Izady, M., Dinarvand, S., Pop, I., & Chamkha, A. J. (2021). Flow of aqueous Fe_2O_3–CuO hybrid nanofluid over a permeable stretching/shrinking wedge: A development on Falkner–Skan problem. *Chinese Journal of Physics*, *74*, 406-420.